Electron spectroscopy of doubly excited states in He produced by slow collisions of He^{2+} ions with Ba atoms

K. Iemura,[1] S. Ohtani,[1] H. Suzuki,[1] J. Takeda,[2] S. Machida,[2] K. Tanabe,[2] T. Takayanagi,[2] K. Wakiya,[2] M. Sekiguchi,[3] Y. Kanai,[5] S. Kitazawa,[6] X. M. Tong,[4] D. Kato,[4] S. Sakaguchi,[5,7] T. Watanabe,[4] and F. J. Currell[8]

[1]*Institute of Laser Science, University Electro-Communications, Chofu, Tokyo, 182-8585, Japan*

[2]*Department of Physics, Sophia University, Chiyoda-ku, Tokyo, 102-8554, Japan*

[3]*Center for Nuclear Study, The University of Tokyo, Wako, Saitama 351-0198, Japan*

[4]*ICORP, Japan Science and Technology Corporation, Axis Chofu 3F, 1-40-2 Fuda Chofu, Tokyo 182-0024, Japan*

[5]*Institute of Physical and Chemical Research (RIKEN), Wako, Saitama 351-0198, Japan*

[6]*Japan Atomic Energy Research Institute, Tokai, Ibaraki 319-1151, Japan*

[7]*Graduate School, Saitama University, Shimookubo, Urawa 338-0825, Japan*

[8]*Department of Physics, The Queen's University of Belfast, Belfast, Northern Ireland, BT7 1NN, United Kingdom*

(Received 7 September 2000; revised manuscript received 16 April 2001; published 16 November 2001)

We measured ejected electron spectra caused by autoionization of doubly excited states in He atoms; the excited He was made by double electron capture of low-energy He^{2+} ions colliding with Ba atoms. Measurements were performed by means of zero degree electron spectroscopy at projectile energies from 40 to 20 keV. Electron spectra due to autoionization from the states $He(2lnl')$ to $He^{+}(1s)$ for $n \geqslant 2$, and those from $He(3lnl')$ to He^{+} $(2s$ or $2p)$ for $n \geqslant 3$, were observed. Line peaks in the spectra were identified by comparing observed electron spectra with those of several theoretical calculations. It was found that doubly excited states of relatively high angular momenta such as the *D* and *F* terms were conspicuously created in a quite different manner from the cases of the production of doubly excited states by the use of photon, electron, or ion impacts on neutral He atoms. Rydberg states with large *n* values were observed with high population in both the $He(2lnl')$ and $He(3lnl')$ series. Other remarkable features in the electron spectra are described and the mechanisms for the production of these electron spectra are discussed qualitatively.

DOI: 10.1103/PhysRevA.64.062709 PACS number(s): 34.70.+e, 32.30.−r, 82.30.Fi

I. INTRODUCTION

Multiply excited states in atoms have been one of the most fascinating research subjects for both experimental and theoretical atomic physicists. Doubly excited states in He are the simplest example of the multiply excited states in atoms and have been studied from the earliest period. Therefore, they are most widely studied and enormous information and knowledge have been obtained in experimental and theoretical investigations.

The earliest experimental observations of the doubly excited states in He were reported in photoabsorption spectra [1] and electron-energy-loss spectra [2], one after another from 1963. The studies on the spectra of ejected electrons due to autoionization of doubly excited He by ion bombardment [3] and electron impact [4–6] followed. Ever since, photoabsorption experiments on He atoms have succeeded in improving the resolution in using several synchrotron radiation facilities [7–9]. Measurements of photoelectron spectra accompanied by photoabsorption were also applied to study the doubly excited states in He [10].

By virtue of photoabsorption spectroscopy in the wavelength region from 19 to 21 nm using synchrotron radiation, the knowledge on spectra of doubly excited states in He has been abundantly supplied over these years. The states were interpreted to be characterized by electron-electron correlations. For example, in the photoabsorption spectra below the $N=2$ threshold, three different series of the $^1P^o$ doubly excited states have been observed, which were specified afterwards as the $_2(0,1)_n^+$, $_2(1,0)_n^-$, and $_2(-1,0)_n^0$ $(n \geqslant 2)$ states using correlation quantum numbers by Herrick and Sinanoglu [11] and by Lin [12]. These experimental observations stimulated theoretical efforts for understanding these characteristics. Many computational methods have been developed to calculate the properties of doubly excited states. A number of classification schemes and appropriate quantum numbers have been proposed. In terms of the quantum numbers, order and regularity in energy levels, in the autoionization and the radiative transition rates of the states became to be described reasonably. The classification schemes and the computational methods for doubly excited states of atoms are reviewed by Lin [13].

In the meantime, some doubly excited states belonging to the $^1S^e$ and $^1D^e$ terms were observed in electron-impact spectra [2] and ejected electron spectra by the use of electron impact [4–6] and ion bombardment [3,14]. The triplet states, such as the $^3P^o$ term, were found to be populated by low-energy electron impact [4,5] or by the bombardment of fast molecular ions [3]. These observations promoted numerical calculations of energy values and autoionization widths of various doubly excited states of different angular momenta and spin states. A large number of calculational results based on various theoretical methods were supplied for the comparisons with experimental data. On the other side, ejected electron spectroscopy due to autoionization of doubly excited states created by electron impact near threshold [15] or by low-energy ion impact [16] were found to be very useful for studying the post collision interaction (PCI) effect.

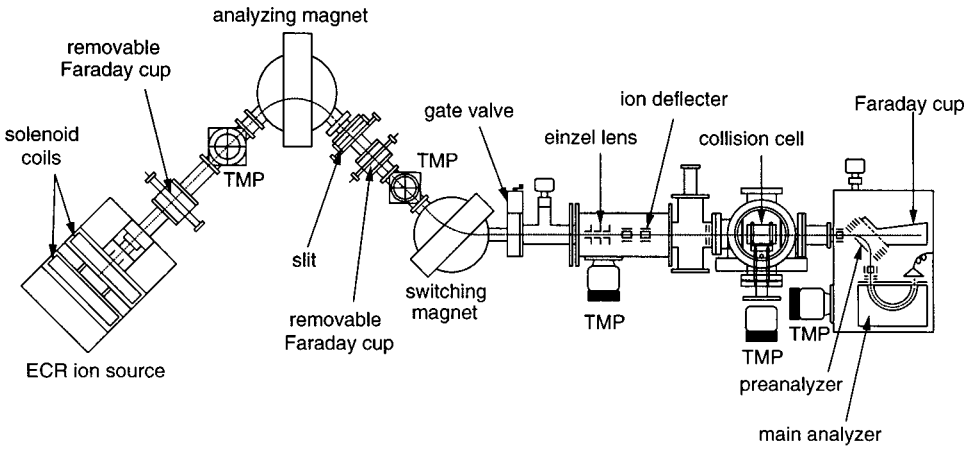

FIG. 1. Schematic diagram showing the experimental arrangement of apparatus. The size of the collision cell and the energy analyzer system are emphasized in comparison with that of the ion source and the ion-beam guiding system.

In recent years, it has been found that doubly excited states may be efficiently populated by double electron-capture processes in low-energy collisions of multiply charged ions with atomic targets. These states are identified by the electron spectra following autoionization from the doubly excited states. Particularly, the doubly excited states in He-like ions or neutral atoms are formed by double electron capture of fully stripped ions from many electron atoms or molecules. Mack *et al.* studied the doubly excited states of the $(3l3l')$ configurations in C^{4+} ions and O^{6+} ions produced by collisions of $C^{6+}+H_2$ and $O^{8+}+He$, respectively, [17]. Sakaue *et al.* studied doubly excited states of the $(2l3l')$ configurations in C^{4+} ions produced by $C^{6+}+He$ collisions [18,19] and in B^{3+} ions produced by $B^{5+}+He$ collisions [20]. Bordenave-Montesquieu *et al.* did similar measurements in He-like N^{5+} ions and Ne^{8+} ions of the $(3lnl')$ configurations by the $N^{7+}+He$ and $Ne^{10+}+He$ collisions, respectively, [21]. Chesnel *et al.* observed the contributions to radiative stabilization in $Ne^{10+}+He$ collisions for the $(3lnl')$ and the $(4lnl')$ configurations [22].

The doubly excited states in neutral He atoms formed by the double electron-capture processes in He^{2+}-neutral atom or He^{2+}-molecule collisions have been studied very scarcely until present days. Moretto-Capelle *et al.* studied the double electron transfer processes in $He^{2+}+Ar$ collisions [23]. Their main interests were, however, not to identify the doubly excited states but to investigate mechanisms of the electron transfer processes. We have been carrying out a series of measurements on the ejected electron spectra due to autoionization from the He doubly excited states. The excited He is produced by 20 to 40 KeV He^{2+} collisions with alkaline-earth atoms, Ba, Sr, Ca, and Mg.

Alkaline-earth atoms can be considered as quasi-two-electron atoms with a paired spin state. Principal quantum numbers n of the outermost orbital correspond to 6, 5, 4, and 3, for Ba, Sr, Ca, and Mg, respectively. We may change the binding energy of the two outermost electrons from 15.2 to 22.7 eV by changing the target species. Furthermore, larger cross sections of the two-electron transfer processes are expected for alkaline-earth atoms relative to rare-gas atoms, because alkaline-earth atoms in the ground state have large polarizabilities in contrast to rare-gas atoms.

A part of the results of these measurements were reported in two international conferences [24,25]. As the first full paper in this series of investigations, we present the results of electron spectra from doubly excited He atoms created by $He^{2+}+Ba$ collisions. Our main interest lies in the identification of the autoionizing states populated by the double electron-capture processes by He^{2+} ions from the quasi-two-electron atoms. Section II gives a brief outline of the experimental apparatus and procedures. Experimental results and discussion are presented in Sec. III, where the electron spectra from the doubly excited He atoms in the $(Nlnl')$ configurations, $n \geqslant N$, $N=2$ and 3, are presented. The identification of most peaks in the spectra are discussed using tables of the energy values and level widths obtained from theoretical calculations. Some remarkable features observed in the population distributions of doubly excited states produced in the present collision system are discussed. The dependence of the population distributions on collision energy is described and the mechanism of the processes are discussed qualitatively. We summarize the contents of this research in Sec. IV.

II. EXPERIMENTAL METHOD

A. Experiment apparatus

A schematic drawing of the experimental setup is shown in Fig. 1. We used the 14.25 GHz ECR (Electron Cyclotron Resonance) ion source at the Center for Nuclear Study, School of Science, the University of Tokyo [26]. It has strong axial and radial magnetic fields whose field strengths are over 10 kG. The diameter of the plasma chamber is 50 mm and the diameter and length of the ECR zone is 30 and 70 mm, respectively. A beam of He^{2+} ions was extracted from the ECR ion source with a voltage of 5 to 20 kV applied on the plasma chamber. Consequently, the kinetic energies of He^{2+} ions were 10 to 40 keV. The He^{2+} ions were selected by a 90° sector magnet analyzer and focused by an einzel lens. The He^{2+} beam current was typically 200–400 μA, as measured just after the charge state analyzer. The beam of He^{2+} ions was further transported through a switching magnet, and focused by an einzel lens to our experimental line. The vacuum in the charge state analyzer and the beam transport system was kept below 10^{-7} Torr.

The ion beam passes through a vapor of samples in a vaporization cell. The vaporization cell of heat pipe structure is 50 mm long and has entrance and exit apertures of 1.0 and 1.5 mm diameter, respectively. In order to stabilize the inner temperature, the cell was installed with three radiation shields. The vapor pressure was estimated from the temperature of the vaporization cell. Measurements were performed at a low-vapor pressure of the order of magnitude 10^{-4} Torr in the vaporization cell, which was considered to assure the single collision condition. The vaporization cell was biased with a negative voltage to extract ejected electrons.

Electrons ejected in the same direction with the ions were measured by the technique of zero-degree electron spectroscopy [27–29]. By virtue of this technique, the Doppler broadening could be minimized and the best energy resolution was expected [30]. Ejected electrons were measured with a combination of a 45° parallel plate electrostatic analyzer and a high-resolution simulated hemispherical-type electrostatic analyzer with a mean radius of 104 mm. The magnetic field inside the collision and analyzing chambers was reduced to a few mG by a mu-metal shielding.

The beam line, the collision chamber, and the analyzing chamber are evacuated by 250 l/s turbo molecular pumps, separately. A cooling trap is mounted around the vaporization cell in the collision chamber. The cooling trap protects the analyzer system from contamination by metal vapor and serves to keep a good vacuum. Typical pressures in the collision chamber and the analyzing chamber were around 10^{-7} and 10^{-8} Torr, respectively.

The 45° parallel plate electrostatic analyzer serves as a preanalyzer to separate the ejected electrons from background electrons and primary He^{2+} ions. Electrons ejected from doubly excited He** atoms formed in the collision cell in the same direction with the primary beam are deflected by a 90° angle and directed into the simulated hemispherical analyzer that serves as a main analyzer. This arrangement proved to be useful to suppress the background noise effectively. The incident ions were practically not deflected and were detected by a Faraday cup located behind the parallel plate preanalyzer. A typical ion current was 100 nA measured at the Faraday cup.

In order to operate the main analyzer in the constant resolution mode, ejected electron spectra were measured by scanning a deceleration voltage applied to the hemispherical analyzer synchronously with the deflection voltage of the 45° parallel plate preanalyzer keeping the electron pass energy in the main analyzer constant. A multichannel analyzer was used in a multiscalar mode to register the number of detected electrons as a function of the electron energy. A signal for advancing the channel and the deceleration voltage was issued at every instant when the integrated ion current on the current integrator reached a definite value. This procedure was useful to prevent the unfavorable influence due to unavoidable changes in the ion current for the correct measurements of the ejected electron intensity. The pass energy was chosen to be about 6 eV during the measurements. The overall energy resolution of the apparatus was estimated to be better than 100 meV full width at half maximum.

B. Transformation from the laboratory frame to the emitter frame

Experimental results give the ejected electron spectra just in the frame of reference fixed to the laboratory, which are influenced by kinematic effects due to the Doppler effect. Because the electrons are emitted from swiftly moving projectile He** atoms formed by the double electron capture in the He^{2+}+Ba collisions, measured energies of emitted electrons include energy shifts and other effects due to the Doppler effect. Therefore, we need to transform the spectra from the laboratory frame to the emitter frame in order to compare with the spectra theoretically calculated.

In the first step, we corrected relative intensities in the spectra in the laboratory frame using a detection efficiency curve as a function of electron energy, which was obtained by additional experimental measurements under the same conditions as that of the present energy analyzer system (see below).

In the second step, we performed the energy transformation to the emitter frame from the laboratory frame simultaneously during the measurement of the individual electron spectra, by applying the specific transforming formula using a computing system. Each measurement was performed after a procedure for the energy calibration, in which the two parameters relevant to the space-charge effect and to the accuracy of the projectile ion energy so that the energy position of the two reference peaks coincide with the adequate theoretical values.

The electron spectra in the emitter frame obtained in this way were corrected concerning the relative intensities by the frame transformation from the laboratory to the emitter frame using a formula representing a relation of double differential cross sections between the laboratory and emitter frames.

We will describe the relation between the laboratory frame and the emitter frame in the present subsection, and succeed to the procedures for the energy calibration and the correction of the relative intensities in the energy spectra in the next subsection.

The relation in the energy of the ejected electron between the laboratory frame and the emitter frame is obtained as follows. The relation in the velocity between projectile ion and ejected electron is presented as $\vec{V}_{\rm lab}=\vec{V}_{\rm ion}+\vec{V}_{\rm emi}$, where $\vec{V}_{\rm lab}$ is the velocity of the ejected electron in the laboratory frame, $\vec{V}_{\rm ion}$ is that of the projectile ion, and $\vec{V}_{\rm emi}$ is that of the ejected electron in the emitter frame. Here, we define the angle between $\vec{V}_{\rm ion}$ and $\vec{V}_{\rm lab}$ as θ. The formula $\vec{V}_{\rm lab}=\vec{V}_{\rm ion}+\vec{V}_{\rm emi}$ is rewritten as

$$V_{\rm emi}^2=V_{\rm lab}^2+V_{\rm ion}^2-2V_{\rm lab}V_{\rm ion}\cos\theta,$$

$$V_{\rm emi}^2=(V_{\rm lab}-V_{\rm ion}\cos\theta)^2+V_{\rm ion}^2\sin^2\theta. \qquad (1)$$

The velocities $V_{\rm emi}$, $V_{\rm lab}$, and $V_{\rm ion}$ correspond to $\sqrt{2E_{\rm emi}/m_e}$, $\sqrt{2E_{\rm lab}/m_e}$, and $\sqrt{2E_{\rm ion}/M_{\rm ion}}$, respectively. Here, m_e and $M_{\rm ion}$ indicate the masses of electron and ion, and $E_{\rm emi}$, $E_{\rm lab}$, and $E_{\rm ion}$ are the energy of the ejected electron in the emitter frame, that of the ejected electron in the

laboratory frame, and that of the projectile ion, respectively. The energy relation between the emitter frame and the laboratory frame is deduced from Eq. (1) as,

$$E_{\mathrm{emi}}=\left(\sqrt{E_{\mathrm{lab}}}-\sqrt{\frac{E_{\mathrm{ion}}}{1823A}}\cos\theta\right)^2+\frac{E_{\mathrm{ion}}}{1823A}\sin^2\theta, \quad (2)$$

where A is the mass number of the projectile ion. The numerical value 1823 is the ratio m_u/m_e, where m_u is the atomic mass unit and m_e is the electron mass. When the direction of the observation is the same as the ion beam, i.e., in the forward direction, $\theta=0°$, Eq. (2) is simply expressed by

$$E_{\mathrm{emi}}=\left(\sqrt{E_{\mathrm{lab}}}-\sqrt{\frac{E_{\mathrm{ion}}}{1823A}}\right)^2. \quad (3)$$

This formula was applied for the transformation from the laboratory frame to the emitter frame for the energy scale.

There is a possibility that the electrons emitted to the opposite direction to the ion-beam travel to the forward direction in the laboratory frame, when the speed of the emitted electrons is lower than that of the ion. In this case, square root of the energy in the laboratory fram, $\sqrt{E'_{\mathrm{lab}}}$ is presented as

$$\sqrt{E'_{\mathrm{lab}}}=\sqrt{\frac{E_{\mathrm{ion}}}{1823A}}-\sqrt{E'_{\mathrm{emi}}}. \quad (4)$$

However, the value of $\sqrt{E'_{\mathrm{lab}}}$ was out of the range of energy we measured through the present experiment, because we measured the electrons of energies higher than the value $E_{\mathrm{ion}}/1823A$ in the laboratory frame, which corresponded to the zero energy value of the forward emitted electrons in the emitted frame. Therefore, we did not need to consider that the signals from the electrons emitted backward gave any effects to the proper measurement of the ejected electron spectra in the forward direction.

C. Energy calibration and correction for the relative intensity

To accumulate signals of energy-analyzed electrons, we used a multichannel analyzer with 1024 channels, each of which corresponded to the deceleration voltage applied to the electron spectrometer. The deceleration voltage also corresponded to the ejected electron energy in the laboratory frame. In order to calibrate the ejected electron energy, two parameters had to be determined for every measurement. The first parameter α is related to the correction factor in the energy of the projectile ion beam, while the second parameter β to the shift of the energy of the ejected electron due to the space-charge effect formed by the ion beam.

The transforming formula Eq. (3) was rewritten as

$$E_{\mathrm{emi}}=(\sqrt{E_{\mathrm{lab}}+\beta}-\sqrt{E_{\mathrm{ion}}\alpha/1823A})^2, \quad (5)$$

for the energy calibration procedure. The parameters α and β were obtained by solving the two-line simultaneous equations produced by applying the two experimental peak values of E_{lab} so that the energies of the corresponding E_{emi} agree with the theoretical energies of the two reference peaks selected for the calibration standards. If the energy of the projectile ions is correctly identical to the accelerating voltage of the ion-beam times electronic charge, α equals to unity. And if the energy shift by the space-charge effect is negligibly small, β would be zero eV. Usually, these parameters were considered to be unchangeable during the measurement of each spectrum. Changes from unity in the values of α stayed within a few percent, and changes in the values of β were within a few eV, for respective measurements of the spectrum.

When both the reference peaks were sharp and clearly defined, the accuracy of the energy was obtained within ±0.02 eV, as the case of the spectra for the $(2lnl')$ configurations, which will be described in the section of the experimental results. However, as for the spectra for the $(3lnl')$ configurations, when the energy of the series limit had to be used as the reference point, the values of α and β depended very sensitively on the applied values for E_{lab} in Eq. (5), and acceptable values of α and β could not be obtained unless the applied values for E_{lab} were correctly chosen. In these cases, accuracy of the energy calibration was estimated to be ±0.03 eV at the best.

In order to obtain the spectra with true relative intensities in the emitter frame from the spectra given by the abovementioned transformation for the energy scale, relative intensities in the spectra had to be corrected using the following two procedures. The first correction was based on the detection efficiency of the energy analyzer as a function of the electron energy. We measured the detection efficiency curve in the present analyzer system by doing an extra experiment for this purpose (see below).

The second one was based on the frame transformation regarding the intensity of the spectra. The ratio of the double differential cross sections between the laboratory frame and the emitter frame was used to calculate the relative intensity in the spectra in the emitter frame. Changes in the relative intensities in the ejected electron spectra in the course of the frame transformation may be accounted for the changes in the relevant solid angles and energy widths between the laboratory frame and the emitter frame. The relation between the laboratory frame and the emitter frame for the double differential cross sections in the electron ejection spectra is represented by the following formula [30],

$$\frac{\partial^2\sigma_{\mathrm{emi}}}{\partial E_{\mathrm{emi}}\partial\Omega_{\mathrm{emi}}}=\left(\frac{E_{\mathrm{emi}}}{E_{\mathrm{lab}}}\right)^{1/2}\frac{\partial^2\sigma_{\mathrm{lab}}}{\partial E_{\mathrm{lab}}\partial\Omega_{\mathrm{lab}}}. \quad (6)$$

We obtained the relative intensities in the electron spectra in the emitter frame by multiplying those of the spectra in the laboratory frame by $(E_{\mathrm{emi}}/E_{\mathrm{lab}})^{1/2}$ at every channel of the multichannel analyzer. By the frame transformation, the peak intensities at lower energies are reduced relative to those of higher-energy peaks. For instance, the reduction ratio of intensity of a peak placed at 4.2 eV to that placed at about 39 eV in the emitter frame is calculated to be about 0.63 when the ion energy is 40 keV.

An extra experiment, mentioned above, was performed to determine the detection efficiency of the present analyzer

system as a function of the energy under the same condition as that for the measurements of all spectra. To do that, the *MNN* Auger electron spectra in Kr and the *NOO* Auger electron spectra in Xe produced by electron impact were observed. The relative intensities in the Auger peaks measured with our analyzer were compared with those available from a paper by Werme, Bergmark, and Siegbahn [31], which has given the correct relative intensities in these Auger electron spectra. The relative detection efficiency decreased from 1.0 to about 0.6 as the energy increased from 14 to 78 eV, which was the practical energy range of the present experiments. Thus, we obtained a formula of the relative detection efficiency of our analyzer by the least squares method from the experimental points as a function of the electron energy.

The relative intensities in the ejected electron spectra in the emitter frame obtained by applying these procedures are considered to be correct within an accuracy of $\pm 30\%$.

III. RESULTS AND DISCUSSION

We have measured ejected electron spectra originating from the autoionization of doubly excited states in He. The excited He atoms were produced by double-electron-capture processes in collisions of He^{2+} ions with Ba atoms, i.e.,

$$He^{2+} + Ba \rightarrow He^{**}(Nlnl') + Ba^{2+}$$
$$\rightarrow He^{+}(N'l'') + Ba^{2+} + e^{-}.$$

Here, $He^{**}(Nlnl')$ indicates the doubly excited He atom with the $Nlnl'$ configurations, and $He^{+}(N'l'')$ indicates the He^{+} ion that keeps the $N'l''$ electron following autoionization. Collision energies were 20, 30, and 40 keV.

A panoramic view of the ejected electron spectra is shown in Fig. 2 for He^{2+}+Ba collisions at ion energies 40 and 20 keV, covering the emitter electron energy from 0 to about 42 eV. In these spectra, the peaks in the energy range from 32 to 42 eV are attributed to autoionization $He^{**}(2lnl') \rightarrow He^{+}(1s)$, where $n \geqslant 2$. On the other hand, the peaks in the energy range 3 to 8 eV are attributable to autoionization $He^{**}(3lnl') \rightarrow He^{+}$ ($2s$ or $2p$), where $n \geqslant 3$. In the energy range from 0 to 3 eV, structures attributable to the autoionization $He^{**}(4lnl') \rightarrow He^{+}(3l'')$ and similar upper series are observed. The energy calibration for these spectra was performed by choosing the $He^{**}(3lnl')$ series limit energy 7.56 eV and the peak energy 38.92 eV from the $He^{**}(2s3p)\,^1D^e$ level as the reference energies for the calibration. The relative intensities in these spectra are corrected by considering the detection efficiency and the frame transformation. The accuracy in the emitter electron energy is estimated within 0.04 eV, and accuracy in the relative intensities is considered to be within 30%.

A. The $2lnl'$ series

The ejected electron spectrum measured in the energy range from 32 to 42 eV is shown in Fig. 3. The spectrum is attributed to the autoionization processes $He^{**}(2lnl') \rightarrow He^{+}(1s)$. The energy scale of the spectra was calibrated by using the autoionization lines of the states

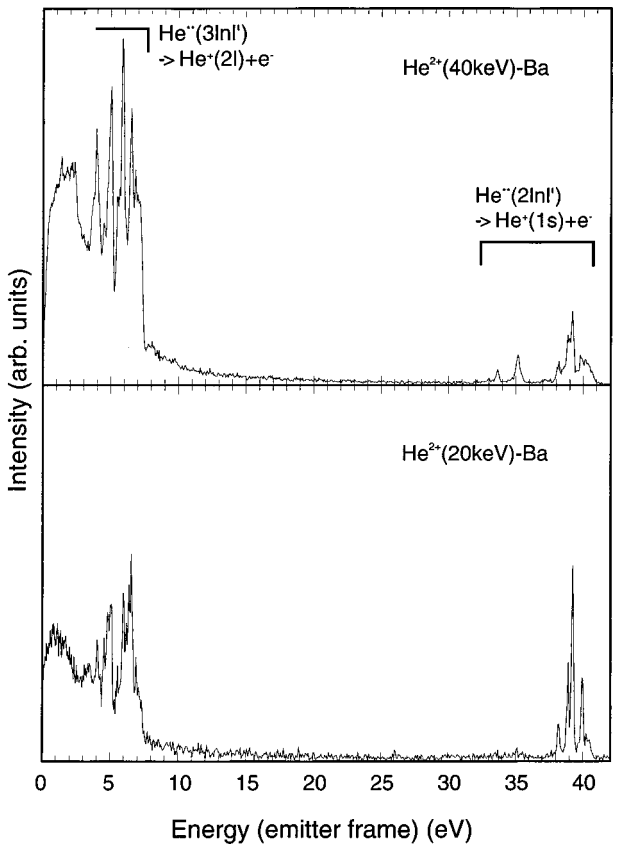

FIG. 2. Ejected electron spectra ranging from 0 to 42 eV that are measured in the forward direction for the He^{2+}+Ba collisions. The ion collision energies are 40 and 20 keV. Relative intensities in the spectra are corrected regarding both the detection efficiency and the frame transformation. The accuracy in the relative intensity is within about 30%. The accuracy in the electron energy covering these spectra is estimated to be about 0.04 eV.

$2s2p\ ^3P^o$(33.72 eV) and $2p3p\ ^1D^e$ (38.92 eV), considering the correction for the PCI shifts of 0.013 and 0.018 eV, respectively.

In Fig. 3, most peaks and bumps are labeled with letters, $a,b,c,\ldots$, for the identification of states in comparison with theory. Table I gives theoretical energies of ejected electrons obtained from the results of calculations for state energies of the doubly excited states in He by Lindroth [32], Ho and Bhatia [33–37], Tang Watanebe, and Matsuzawa [38,39] and Morishita *et al.* [40], and Lipsky, Amania, and Conneely [41]. To represent the states, we use the notation ${}_N(K,T)_n^{A\ 2S+1}L^{\Pi}$ by the hyperspherical classification scheme of Lin [12,13], where n is the principal quantum number of the outer electron, N being that of the inner electron, and K, T, and A are the correlation quantum numbers, while L, S, and Π are the usual quantum numbers. Single-particle notation for the electron configuration, such as $(Nlnl')$ are used in addition because of its common use. States of the P^e and D^o terms have not been listed in Table I, because these states are nonautoionizing.

Energy values of the peaks and bumps read from the experimental spectra are tabulated in line with the theoretical energies in Table I. The accuracy of the experimental energy

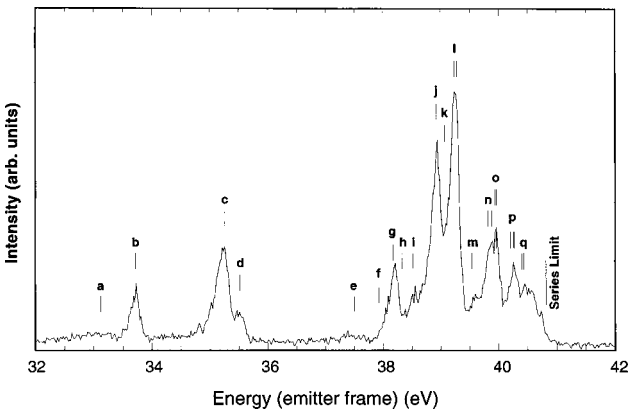

FIG. 3. Typical ejected electron spectrum from the doubly excited states He**$(N=2)$ in the forward direction, which are produced by the He^{2+}+Ba collisions of 40 keV ion energy. Alphabetical notations indicate corresponding doubly excited states. Vertical short lines indicate the theoretical energies, for which the PCI shifts calculated using the linewidth, are included. Reference peaks for the energy calibration was chosen at *b*, the $_2(1,0)_2^+\ ^3P^o$ state (33.72 eV), and at *j*, the $_2(1,0)_3^+\ ^1D^e$ state (38.92 eV). Accuracy in the electron energy is within 0.02 eV.

values is estimated to be ± 0.02 eV. The PCI shifts of the peak energy calculated using the theoretical lifetime for the respective states are indicated in Table I, when they are larger than 0.01 eV. Vertical lines in Fig. 3 represent the theoretical energies, some of which are corrected with the calculated PCI shift. The experimental energy values of peaks agree with the corresponding theoretical ones within the experimental uncertainties, if the PCI shifts are considered.

The energy positions of the ejected electrons are considered to be shifted to the low-energy side due to the PCI effect. This is originated by the Coulomb interaction between the autoionized electron and the doubly charged ion formed from the target atom after the double-electron transfer collision. The line shape and the energy shift in the ejected electron spectra due to the PCI effect are dependent on the ejection angle with respect to the incident ion direction, therefore, the simple formula of Rarker and Berry [16] is not valid for the present experimental arrangement. We use the formula by Boudjema *et al.* [42] for the distribution function $F(\varepsilon)$ to obtain the line shape in terms of electron energy ε and the energy shift $\Delta\varepsilon=\varepsilon-E$, where E is the intrinsic energy of the ejected electron:

$$F(\varepsilon)=b\,\frac{\xi q\Gamma/v_i}{(\Delta\varepsilon^2+\Gamma^2/4)}\,\frac{\exp[(2\xi q/v_i)\tan^{-1}(\Gamma/2\Delta\varepsilon)]}{1-\exp(-2\pi\xi q/v_i)}, \tag{7}$$

where q is the charge of the target ion after the collision, Γ is the width of the autoionizing state, and v_i is the speed of the projectile ion. The factor ξ is given by van der Straten and Morgenstern [43] as

$$\xi=1-\frac{V}{|\vec{V}-\vec{v}_0|}, \tag{8}$$

where $\vec{v}_0$ is the velocity vector of the electron, and $\vec{V}$ is the velocity vector of perturber ion (the target ion formed after the collision), both in the emitter frame (attached to the incident ion). Thus, $\vec{V}=-\vec{v}_i$, where $\vec{v}_i$ is the velocity vector of the projectile. The energy shift for each peak position was obtained from the distribution function calculated using theoretical widths of the relevant states for a collision energy of 40 keV.

As shown in Table I and Fig. 3, peaks with label letters *a* to *e* are classified as $(2l2l')$ states. Peaks with letters *f* to *l* (l_1 and l_2) are classified as $(2l3l')$ states, peaks with letters *m* to *o* (o_1,o_2,o_3) as $(2l4l')$, peaks with *p* (p_1,p_2,p_3) as $(2l5l')$, and peaks with $q(q_1,q_2,q_3)$ as $(2l6l')$, and so on. The series limit of the $(2lnl')$ states is indicated by a vertical line at 40.81 eV.

In the region for states of the $(2l2l')$ configuration, autoionization lines from the states $_2(1,0)_2^+\ ^3P^o$ (label *b*), $_2(1,0)_2^+\ ^1D^e$ (label *c*), and $_2(0,1)_2^+\ ^1P^o$ (label *d*) are conspicuous, where the line from the $^1D^e$ state is outstanding. In contrast, states of the $^1S^e$ term (label *a* and *e*) appear only very weakly.

In the region for the $(2l3l')$ states, lines from the states $_2(1,0)_3^-\ ^1P^o$ (label *g*), $_2(1,0)_3^+\ ^3P^o$ (label *i*), $_2(1,0)_3^+\ ^1D^e$ (label *j*), and $_2(1,0)_3^0\ ^1F^o$ (label l_1), $_2(0,1)_3^0\ ^1D^e$ (label l_2) are conspicuous, where l_1 and l_2 are unresolved due to the lack of the resolving power of the spectrometer. The $_2(0,1)_3^+\ ^1P^o$ state (label *k*) is placed between the line *j* and line $l_{1,2}$ and does not form a peak. It is worth noticing that lines from the states $_2(1,0)_3^+\ ^1D^e$ (label *j*), $_2(1,0)_3^0\ ^1F^o$ (label l_1), and $_2(0,1)_3^0\ ^1D^e$ (label l_2) have the largest intensities eminently over the whole range in the spectra.

In the region for the $(2l4l')$ states, the states $_2(1,0)_4^-\ ^1P^o$ (label *m*), $_2(1,0)_4^+\ ^1D^e$ (label *n*), and $_2(1,0)_4^0\ ^1F^o$ (label o_1), and $_2(0,1)_4^0\ ^1D^e$ (label o_2) are conspicuous. In the region for the $(2l5l')$ states, the states $_2(1,0)_5^+\ ^1D^e$, $_2(1,0)_5^0\ ^1F^o$, and $_2(0,1)_5^0\ ^1D^e$ appear to form a single peak (label *p*). Similarly, in the region for the $(2l6l')$ states, the states $_2(1,0)_6^+\ ^1D^e$, $_2(1,0)_6^0\ ^1F^o$, and $_2(0,1)_6^0\ ^1D^e$ appear to form a single peak (label *q*).

It is worth mentioning that the intensity of autoionization lines for high *n* numbers does not decrease rapidly and then the spectral profile forms a sharp cliff at the series limit of 40.81 eV. This intensity distribution suggests to us that the high-*n* Rydberg states are preferably populated in the process taking place for the present system.

It is a remarkable feature in the present electron spectra that the doubly excited states of high-angular momenta such as the terms ^1D, ^1F are dominantly created, and this feature is quite characteristic for electron-capture processes by highly charged ions from neutral atomic targets. This feature appears in clear contrast with respect to the ejected electron spectra produced by electron- or singly-charged ion impact on neutral He atoms. There, the peaks from the states of ^1P and ^1S terms are dominant, and the intensity of Rydberg states decreases steadily with the quantum number *n* of the outer electron.

TABLE I. Ejected electron energies resulted from autoionization $He^{**}(2lnl') \rightarrow He^{+}(1s)+e^{-}$. Theoretical energies are deduced from the state energies calculated by Lindroth [32], Ho and Bhatia [33–37], Tang, Watanabe, and Matsuzawa [38,39], and Lipsky, Anania, and Conneely [41]. Widths of energy levels are given under the respective electron energies. Figures in the brackets represent the power indices of ten. Observed energies are involved in experimental uncertainties ±0.02 eV and the PCI shift.

Lavel letter	Single-particle notation	State symbol $_N(K,T)^A_n$	State symbol ^{2s+1}L	Theoretical energies (eV) widths Γ (eV) Lindroth	Ho	Tang	Lipsky	Observed values (eV)	PCI shift (−eV)
a	$2s^2$	$_2(1,0)^+_2$	$^1S^e$	33.255	33.255	33.267	33.324	33.25	0.13
				1.236[−1]	1.23[−1]	1.24[−1]			
b	2*s*2*p*	$_2(1,0)^+_2$	$^3P^o$	33.728	33.727	33.726	33.786	33.72	0.01
				8.14[−3]	8.13[−3]	8.14[−3]			
c	$2p^2$	$_2(1,0)^+_2$	$^1D^e$	35.322	35.320	35.323	35.440	35.26	0.07
				6.426[−2]	6.427[−2]	6.47[−2]			
d	2*s*2*p*	$_2(0,1)^+_2$	$^1P^o$	35.561	35.559	35.564	35.688	35.5	0.04
				3.736[−2]	3.736[−2]	3.68[−2]			
e	$2p^2$	$_2(-1,0)^+_2$	$^1S^e$	37.498	37.497	37.500	37.681	37.49	
				5.88[−3]	5.87[−3]	5.95[−3]			
f	2*p*3*p*	$_2(1,0)^-_3$	$^3S^e$	37.924		38.025	38.036		
				1.81[−4]		5.02[−5]			
g	*sp*23−	$_2(1,0)^-_3$	$^1P^o$	38.174	38.173	38.171	38.187	38.2	
				1.04[−4]	1.05[−4]	1.06[−4]			
h	2*s*3*s*	$_2(1,0)^+_3$	$^1S^e$	38.370	38.368	38.367	38.416	38.38	0.04
				3.70[−2]	3.67[−2]	3.70[−2]			
i	*sp*23+	$_2(1,0)^+_3$	$^3P^o$	38.512	38.510		38.546	38.52	
				2.24[−3]	2.24[−3]				
j	2*p*3*p*	$_2(1,0)^+_3$	$^1D^e$	38.934	38.931	38.930	38.972	38.92	0.02
				1.51[−2]	1.51[−2]	1.53[−2]			
k	*sp*23+	$_2(0,1)^+_3$	$^1P^o$	39.072	39.070	39.070	39.012		0.01
				8.19[−3]	8.19[−3]	8.16[−3]			
l_1	2*p*3*d*	$_2(1,0)^0_3$	$^1F^o$	39.230			39.237	39.23	
				3.48[−4]					
l_2	2*s*3*d*	$_2(0,1)^0_3$	$^1D^e$	39.280	39.279	39.278	39.295		
				5.44[−4]	5.47[−4]	5.43[−4]			
	2*p*3*p*	$_2(-1,0)^+_3$	$^1S^e$	39.507	39.506		39.537		
				2.07[−3]	2.12[−3]				
	2*p*3*d*	$_2(-1,0)^0_3$	$^1P^o$		39.530		39.540		
					2.18[−7]				
m	*sp*24−	$_2(1,0)^-_4$	$^1P^o$	39.534	39.549		39.557	39.55	
				2.7[−6]	4.10[−7]				
n_1	2*p*4*p*	$_2(1,0)^+_4$	$^1D^e$		39.815		39.833	39.85	
					6.34[−3]				
n_2	*sp*24+	$_2(0,1)^+_4$	$^1P^o$		39.879		39.877		
o_1	2*p*4*d*	$_2(1,0)^0_4$	$^1F^o$				39.941	39.96	
o_2	2*s*4*d*	$_2(0,1)^0_4$	$^1D^e$		39.957		39.961		
					1.50[−4]				
	*sp*25−	$_2(1,0)^-_5$	$^1P^o$		40.071		40.076		
p_1	2*p*5*p*	$_2(1,0)^+_5$	$^1D^e$		40.019		40.205		
	*sp*25+	$_2(0,1)^+_5$	$^1P^o$		40.229		40.236	40.26	
p_2	2*p*5*d*	$_2(1,0)^0_5$	$^1F^o$				40.259		
p_3	2*s*5*d*	$_2(0,1)^0_5$	$^1D^e$				40.269		
	*sp*26−	$_2(1,0)^-_6$	$^1P^o$		40.326		40.328		
q_1	2*p*6*p*	$_2(1,0)^+_6$	$^1D^e$				40.398		
	*sp*26+	$_2(0,1)^+_6$	$^1P^o$		40.413		40.417	40.45	
q_2	2*p*6*d*	$_2(1,0)^0_6$	$^1F^o$				40.430		
q_3	2*s*6*d*	$_2(0,1)^0_6$	$^1D^e$				40.436		

On the other hand, studies on the ejected electron spectra produced by collisions of fully stripped ions B^{5+} [20], C^{6+} [17–19], N^{7+} [21], O^{8+} [17], and Ne^{10+} [21,22] with He atoms or H_2 molecules have generally demonstrated the remarkable tendency that the population of doubly excited states in He-like ions with high-angular momentum terms are predominant.

As for the $(2lnl')$ series, Sakaue and Ohtani *et al.* [18–20] have reported the electron spectra due to autoionization of the $(2l2l')$ and $(2l3l')$ states in B^{3+} ions, and the $(2l3l')$ states in C^{4+} ions, both with identification of major peaks. The basic feature in the population distribution, where the ${}_2(1,0)_2^+\,{}^1D^e$, ${}_2(1,0)_3^+\,{}^1D^e$, ${}_2(1,0)_3^0\,{}^1F^o$, and ${}_2(0,1)_3^0\,{}^1D^e$ states are dominant is essentially the same as that found in the present measurement. Moreover, the ${}_2(1,0)_3^-\,{}^1P^o$ state, which is commonly known as the $(sp23\text{-})^1P$ state and is usually observable only very weakly by photoabsorption spectroscopy or other methods, also clearly observed.

There is one distinct difference, however, between the two studies, i.e., the appearance of the peak attributable to the ${}_2(1,0)_2^+\,{}^3P^o$ state in the present experiment; a peak attributable to the ${}_2(1,0)_3^+\,{}^3P^o$ is also observed in the present spectra. In order to rule out the possibility that the occurrence of the triplet states results from a double collision process, we have checked the pressure dependence of the intensity distribution of the peaks and confirmed that the intensity of the peak of the triplet state relative to that of other peaks was independent of the target pressure in the pressure range used. The triplet states were observed only for Ba and Sr, but was not for Ca and Mg. At the moment, we have no definite explanation for this phenomenon. It might be caused by a failure of the *LS* coupling scheme, for the heaviest target atoms. Otherwise, a capture process from the inner shell of the Ba or Sr targets to He^{2+} must be considered unless the spin change occurs.

B. The $3lnl'$ series

The ejected electron spectrum measured in the energy range from 0 to 10 eV is shown in Fig. 4. The spectra are attributed to the autoionization processes $He^{**}(3lnl') \rightarrow He^+$ $(2s$ or $2p)$ and $He^{**}(4lnl') \rightarrow He^+(3l'')$. The electron signals due to the autoionization $He^{**}(3lnl') \rightarrow He^+(1s)$, which are expected to be located in a region from 44.8 to 48.4 eV, have been observed only very weakly. Autoionization signals due to the channel $He^{**}(4lnl') \rightarrow He^+(2l'')$, which are expected from 8.3 to 10.2 eV, have been observed also only very weakly. The energy scale of the spectrum was calibrated by setting the series limit of the $(3lnl')$ states at (7.56 eV), and that of the $(4lnl')$ states at (2.65 eV).

Most peaks and bumps are labeled alphabetically, and their energy values read from the spectra are tabulated corresponding to the symbols of the doubly excited states given in Table II. The accuracy of the experimental energy values is estimated to be ± 0.03 eV. Theoretical energy values of ejected electrons obtained from the results of calculations for state energies by Lindroth *et al.* [32], Ho and Bhatia [44–51], Tang, Watanabe, and Hatsuzawa [38,39], and Koyama *et al.* [52], Koyama, Takafuji, and Matsuzawa [53], and Lipsky, Anania, and Conneely [41] are shown for comparison. The PCI shifts for the ejected electron energies calculated using the theoretical linewidths are listed in the last column, if they are larger than 0.01 eV.

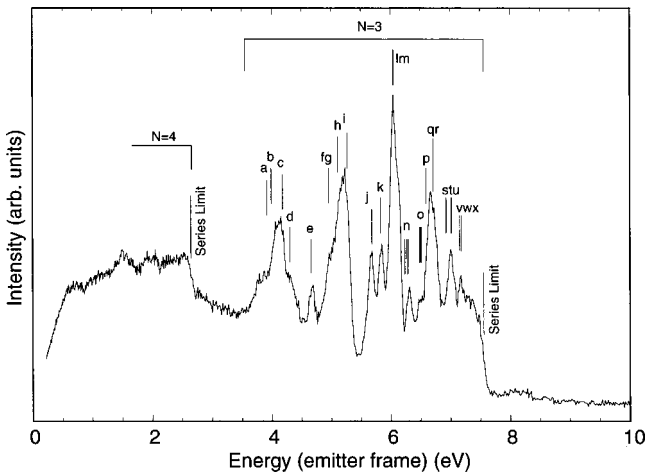

FIG. 4. Typical ejected electron spectrum from the doubly excited states $He^{**}(N=3)$ in the forward direction, which are produced by the He^{2+}+Ba collisions of 40 keV ion energy. Alphabetical notations indicate corresponding doubly excited states. Vertical short lines indicate the theoretical energies, for which the PC shifts calculated using the linewidth, were included. The energy calibration was performed by choosing the two reference energies at the $He^{**}(3lnl') \rightarrow He^+(2l)$ series limit, 7.56 eV, and the $He^{**}(4lnl') \rightarrow He^+(3l)$ series limit, 2.65 eV. Accuracy in the electron energy is estimated to be about 0.03 eV.

Short vertical lines in Fig. 4 represent the theoretical energies corrected with the calculated PCI shifts. As shown in Fig. 4 and Table II, peaks with label letters *a* to *j* are classified as the $(3l3l')$ states. Peaks with letters *k* to *p* are classified as the $(3l4l')$ states; peaks with letters *q* to *s* as $(3l5l')$, peaks with letters *t* to *v* as $(3l6l')$, and peaks with letters *w* and *x* as $(3l7l')$, and so on. The series limit of the $(3lnl')$ states is indicated by a vertical line at 7.56 eV.

In the region for the states of the $(3l3l')$ configuration, the lines involving the states ${}_3(2,0)_3^+\,{}^1S^e$ (label *a*), ${}_3(2,0)_3^+\,{}^3P^o$ (label *b*), ${}_3(2,0)_3^+\,{}^1D^e$ (label *c*), and ${}_3(1,1)_3^+\,{}^1P^o$ (label *d*) are affected by considerable PCI shifts and broadening, forming a single broad peak with bumps on both shoulders. The central peak is caused by the ${}^1D^e$ state. A fine line with label *e* seems to identify the ${}_3(1,1)_3^+\,{}^1D^o$ state. The ${}^1D$ odd states should be nonautoionizing for symmetry reasons in the case of the $(2lnl')$ states, because they have only the $He^+(1s)$ decay channel. However, the corresponding states in the $(3lnl')$ configuration have the decay channel $He^+(2p)$ in addition to $He^+(2s)$, therefore, they become autoionizing. A large peak around 5.2 eV with a tail to the low-energy side is regarded to consist of the states ${}_3(0,0)_3^+\,{}^1S^e$ (label *f*), ${}_3(0,2)_3^+\,{}^1D^e$ (label *g*), ${}_3(2,0)_3^+\,{}^1G^e$ (label *h*), and ${}_3(1,1)_3^+\,{}^1F^o$ (label *i*). Lines due to the ${}^1D^e(g)$, ${}^1G^e(h)$, and ${}^1F^o(i)$ states suffer considerable PCI shifts and broadening, and merge into a single peak. A con-

TABLE II. Ejected electron energies resulted from autoionization $He^{**}(3lnl') \rightarrow He^{+}(2s \text{ or } 2p) + e^{-}$. Theoretical energies are deduced from the state energies calculated by Lindroth [32], Ho Callaway and Bhatia [44–50], Koyama *et al.* [52,53] and Lipsky Anania, and Conneely [41]. Widths of energy levels are given under the respective electron energies. Figures in the brackets represent the power indices of ten. Observed energies are involved in experimental uncertainties ±0.03 eV and the PC shift.

Lavel letter	Single-particle notation	State symbol $_N(K,T)^A_n$	State symbol ^{2s+1}L	Theoretical energies (eV) widths Γ (eV) Lindroth	Ho	Koyama	Lipsky	Observed values (eV)	PCI shift (−eV)
a	$3s^2$	$_3(2,0)^+_3$	$^1S^e$	3.988	3.988	3.988	3.978		0.06
				8.19[−2]	8.16[−2]	8.27[−2]		3.80	
b	$3s3p$	$_3(2,0)^+_3$	$^3P^o$	4.074	4.074		4.052		0.06
					8.09[−2]				
c	$3p^2$	$_3(2,0)^+_3$	$^1D^e$	4.270	4.270	4.272	4.245	4.15	0.11
					1.43[−1]	1.45[−1]			
d	$3s3p$	$_3(1,1)^+_3$	$^1P^o$	4.475	4.476	4.474	4.492	4.25	0.14
					1.90[−1]	1.90[−1]			
e		$_3(1,1)^+_3$	$^1D^o$	4.677	4.677		4.661	4.70	
					8.73[−3]				
f	$3p^2$	$_3(0,0)^+_3$	$^1S^e$	4.970	4.970	4.978	5.024		0.14
					1.81[−1]			4.96	
g	$3s3d$	$_3(0,2)^+_3$	$^1D^e$	5.022	5.022		5.049		0.09
					1.17[−1]				
h	$3d^2$	$_3(2,0)^+_3$	$^1G^e$	5.252	5.253			5.09	0.14
					1.82[−1]				
i	$3p3d$	$_3(1,1)^0_3$	$^1F^o$	5.330	5.329		5.339	5.24	0.07
					8.57[−2]				
j	$3p3d$	$_3(0,0)^+_3$	$^1D^e$	5.715	5.718		5.713	5.69	0.03
					3.26[−2]				
k	$sp34-$	$_3(2,0)^-_4$	$^1P^o$		5.828	5.823	5.829	5.85	
					7.62[−4]	1.90[−3]			
	$3p3d$	$_3(-1,1)^+_3$	$^1P^o$	5.912	5.912	6.009	5.934		0.03
					3.95[−2]	3.35[−2]			
	$3s4s$	$_3(2,0)^+_4$	$^1S^e$		5.958	6.023	5.964		
					1.4[−4]				
l	$3s4f$	$_3(2,0)^-_4$	$^1F^o$		6.044		6.047		
					2.45[−3]			6.05	
m	$3p4p$	$_3(2,0)^+_4$	$^1D^e$		6.104		6.097		0.05
					6.52[−2]				
n	$sp34+$	$_3(1,1)^+_4$	$^1P^o$		6.232	6.235	6.241		0.07
					8.43[−2]	8.13[−2]			
n′		$_3(0.2)^-_4$	$^1D^0$		6.269		6.272	6.32	
n″			$^1{}_{F^e}$		6.301		6.302		
n‴		$_3(1,1)^+_4$	$^1D^o$		6.302		6.303		
		$_3(0,0)^-_4$	$^1P^o$		6.325	6.359	6.329		
			$^1S^e$		6.438		6.455		
o	$3s4d$	$_3(0,2)^+_4$	$^1D^e$		6.470		6.480		
o′			$^1G^e$		6.484				
o″			$^1G^o$		6.490			6.5	
o‴	$3p4g$	$_3(0,2)^0_4$	$^1F^o$		6.505		6.514		
o⁗		$_3(-1,1)^0_4$	$^1F^e$		6.507		6.510		
			$^1P^e$		6.551				

TABLE II. (*Continued*).

Lavel letter	Single-particle notation	State symbol $_N(K,T)^A_n$	State symbol ^{2s+1}L	Theoretical energies (eV) widths Γ (eV) Lindroth	Ho	Koyama	Lipsky	Observed values (eV)	PCI shift (−eV)
p	$3p4d$	$_3(1,1)^+_4$	$^1F^o$		6.591		6.592	6.59	
		$_3(2,0)^-_5$	$^1P^o$		6.603	6.613			
		$_3(0,0)^+_4$	$^1S^e$		6.605	6.601			
			$^1G^e$		6.664				
		$_3(0,0)^+_4$	$^1D^e$		6.681		6.682		
			$^1P^e$		6.706		6.709		
q		$_3(2,0)^-_5$	$^1F^o$		6.712		6.714	6.73	
r		$_3(2,0)^+_5$	$^1D^e$		6.717		6.714		
			$^1D^o$		6.731		6.733		
		$_3(1,1)^-_4$	$^1D^e$		6.760		6.762		
		$_3(-1,1)^+_4$	$^1P^o$		6.762	6.667	6.766		
			$^1F^o$		6.766		6.767		
		$_3(1,1)^+_5$	$^1P^o$		6.784	6.816	6.794		
			$^1F^e$		6.809		6.839		
		$_3(-1,1)^0_4$	$^1D^e$		6.815		6.817		
			$^1F^e$				6.924		
s	$3p5d$	$_3(1,1)^+_5$	$^1F^o$		6.943		6.966	6.94	
			$^1P^o$				6.957		
	$3s5d$	$_3(0,2)^+_5$	$^1D^e$				7.009		
t	$3p6p$	$_3(2,0)^+_6$	$^1D^e$				7.014	7.00	
u	$3s6f$	$_3(2,0)^-_6$	$^1F^o$				7.020		
v	$3p6d$	$_3(1,1)^+_6$	$^1F^o$				7.156	7.14	
w	$3p7p$	$_3(2,0)^+_7$	$^1D^e$				7.181	7.18	
x	$3s7f$	$_3(2,0)^-_7$	$^1F^o$				7.185		

tribution from the $^1S^e(f)$ state is considered to be small. Autoionization of the $_3(0,0)^+_3\ ^1D^e$ state forms a sharp single peak (label *j*).

The energy values of the peak positions experimentally observed agree with the theoretical energies corrected with the PCI shifts within the experimental uncertainty. However, the energy values for most bumps do not agree well with the theoretical energies for the corresponding states even though the correction for PCI shifts are given. This situation may be mainly caused by the overlapping of numerous spectral lines, each of which produces a respective asymmetric profile with a tail toward the low-energy side by the PCI effect.

There is a possibility that the peak labeled by *k* might be identified with the $_3(-1,1)^+_3\ ^1P^o$ state, however, we identify it to otherwise as follows.

In the region for the $(3l4l')$ states, peaks due to the states $_3(2,0)^-_4\ ^1P^o$ (label *k*), $_3(2,0)^-_4\ ^1F^o$ (label *l*), and $_3(2,0)^+_4\ ^1D^e$ (label *m*) are conspicuous. A peak due to the states $^1F^o$ and $^1D^e$ (label *l* and *m*) is the most prominent over the whole region of the $(3lnl')$ series. Around the energy position indicated by label *n*, there are four candidate states that belong to the ^1P, ^1D, and ^1F terms, as shown in Table II. Around the position indicated by label *o*, there are five candidates that belong to ^1D, ^1F, and ^1G terms.

In the region for the $(3l5l')$ states, the main peak appears to consist of the $_3(2,0)^-_5\ ^1F^o$ (label *q*) and the $_3(2,0)^+_5\ ^1D^e$ (label *r*) states. In the $(3l6l')$ region, the main peak is formed by the $_3(2,0)^+_6\ ^1D^e$ (label *t*) and the $_3(2,0)^-_6\ ^1F^o$ (label *u*) states. In the $(3l7l')$ region, the main peak is formed by the $_3(2,0)^+_7\ ^1D^e$ (label *w*) and $_3(2,0)^-_7\ ^1F^o$ (label *x*) states. As for the series $_3(1,1)^+_n\ ^1F^o$ ($n=3,4,5,6$), indicated by labels *i*, *p*, *s*, and *v* the extent of their contribution cannot be judged yet. In addition to these states, level energies of more than twenty $(3l5l')$ states belonging to the ^1D, ^1F, and ^1G terms have been calculated by Ho and Callaway [45] and Lipsky, Anania, and Conneely [41]. We have no information yet about the contribution of these states to the spectral features.

Only few experimental investigations are available on doubly excited states in He, transitions to which are optically forbidden from the ground state, in the energy region of the $(3lnl')$ configurations or higher, using the methods of electron or ion collisions with neutral He atoms. Brotton *et al.* measured the electron energy-loss spectra of He in the energy-loss region from 69 to 72 eV, and deduced energy values and widths of eleven optically forbidden doubly excited states below the $N=3$ threshold [54]. Appearance of the population distribution in these spectra are largely different from the present results, although the measured energies are in good agreement with the present ones.

We may compare our results for the identification of the autoionization lines for the $(3l3l')$ states with that of Mack

et al. [17]. They have reported the spectra due to the doubly excited C^{4+} states produced by the $C^{6+}+H_2$ collision, and those due to the doubly excited O^{6+} produced by the $O^{8+}+He$ collision. In both cases, they have displayed spectra from states with the $(3l3l')$ configurations and given the identification of all lines. There is a good agreement between the present results and theirs, although there are some differences in the intensity distribution. For instance, the peak due to the ${}_3(1,1)_3^+ {}^1D^o$ shows the highest intensity for both the doubly excited C^{4+} and O^{6+} ions.

It should be also mentioned that the intensities of autoionization peaks for high n quantum numbers do not decrease rapidly and, on the contrary, form a sharp edge at the series limit at 7.56 eV. It is observed that states of n around 4 or 5 and of the D, F, or G terms are most preferably populated for the states with the $(3lnl')$ configurations.

We find a clear series limit for the $(4lnl')$ states at 2.65 eV. The peak structure due to the autoionization $He^{**}(4lnl') \rightarrow He^{+}(3l'')$ may not however, be observed clearly. This is probably attributable to the situation that this series overlaps with that due to the autoionization $He^{**}(5lnl') \rightarrow He^{+}(4l'')$.

C. Collision energy dependence of the intensity ratios in the spectra

In the present measurements, the intensities in the spectra were normalized with the target thickness and the beam currents. As shown in Fig. 2, the intensity of autoionization peaks from the $He^{**}(2lnl')$ states is generally weaker than that from the $He^{**}(3lnl')$,$(4lnl')$ and higher excited states for the collision energies between 40 and 20 keV. As the collision energy decreases, the intensities of the peaks due to the $(3lnl')$ and higher excited states relative to those due to the $(2lnl')$ states decrease.

Figure 5 shows the energy dependence of the spectra that belong to the $(2lnl')$ states. The intensities of peaks from the $(2l2l')$ states decrease as the collision energy decreases relative to those from the $(2lnl')$, $n \geqslant 3$, states. The peaks from the $(2l3l')$ and $(2l4l')$ states become prominent and peak shapes appear to be sharper. These phenomena are regarded to be due to the fact that the states of the ${}^1F^o$ term (l_1 and o_1) become more favorable than those of the ${}^1D^e$ terms (j, l_2, n, and o_2) for lower-energy collisions. Meanwhile, the relative intensities from Rydberg series of higher n decrease as the collision energy decreases, and the profile of the spectra near the series limit changes to be a gentle slope instead of a steep cliff.

D. Mechanism of production of doubly excited states by the double-electron transfer process

In order to explain the characteristic features in the production of doubly excited states in He by double-electron transfer collisions of He^{2+} with alkaline-earth atoms, a series of theoretical studies are in progress based on the scheme of analyses using the potential curve crossing, like the Fano-Lichten or the Barat-Lichten theorem. For the potential energy diagram of the $(He\text{-}Ba)^{++}$ system, the essential character of this system is the larger magnitude of the polarizability of the Ba atom as well as that of the doubly excited He atom. The polarizability of excited He states have been calculated by linear response theory based on the density-functional approach. Results of this study have been reported at an international conference [25,55]. Discussions based on the theoretical analyses of potential energy curves to explain the dynamics of the experimental observations will be given in a future publication.

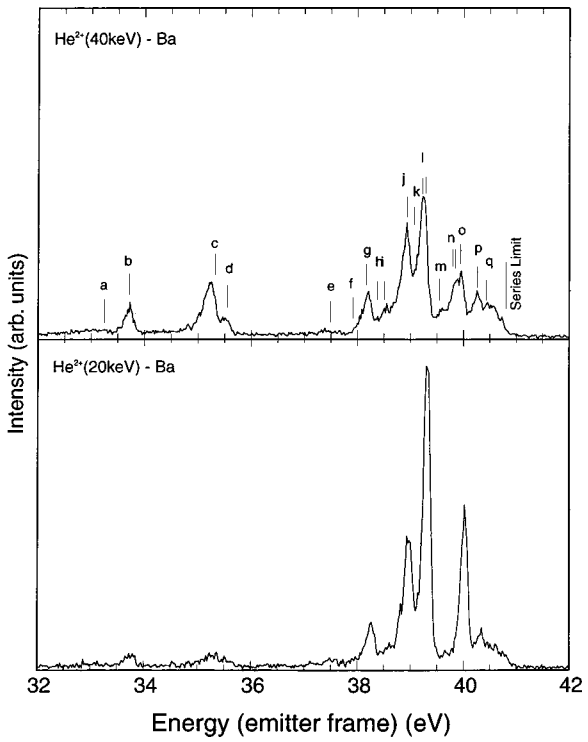

FIG. 5. Comparisons of typical ejected electron spectra between the ion energies 40 and 20 keV. The spectra are from the doubly excited states $H^{**}(N=2)$ in the forward direction, which are produced by the $He^{2+}+Ba$ collisions.

E. Limitation of application of the method of zero-degree electron spectroscopy

There is an intrinsic difficulty in the method for the determination of energy levels of excited He** with high accuracy using the double-electron capture collision by He^{2+} with target atoms. First of all, the autoionization lines suffer from a considerable Doppler shift and broadening because the emitter itself moves rather swiftly. In order to minimize the effect of the Doppler broadening, the zero-degree arrangement for spectroscopy is regarded to be the best choice. The PCI effect that affects the autoionization event in the field of the receding target ion produces a unique profile and shift in particular autoionization lines. The PCI effect causes the overlap of lines and makes the energy determination more difficult, which is especially serious for states of short lifetime (large-energy width) and for low-energy collisions.

We have another problem to ask whether the intensity ratios in the autoionization spectra we have obtained by means of the zero-degree electron spectroscopy really repre-

sent the true distribution of population of doubly excited states in He produced in the collision process of interest. Chen and Lin studied the ejected electron spectra of doubly excited states in He-like ions resulting from double-electron-capture collisions of fully stripped ions by theoretical calculations [56]. They found that the intensity distribution of autoionization lines depended sensitively on the electron ejection angle, and spectra measured at 0° did not generally represent the overall distribution of individual states populated in the collision process. According to their results, the intensity distribution measured at 0° should reflect the contribution from the components of the states for the magnetic quantum number $M=0$, for the autoionization $C^{4+}{}^{**}(2lnl')\rightarrow C^{5+}(1s)$ resulting from $C^{6+}+He$ collisions, because the quantization axis is taken in coincidence with the axis of the quasimolecule created during the collision process. Consequently, the intensity distribution in the spectra measured by the zero-degree arrangement should be interpreted as the distribution of the quantity $(2L+1)\times$(Auger yield)$\times$(production cross section for the $M=0$ component of the excited states). As a result, we should consider a certain tendency that line intensities from high-angular momentum states are emphasized too much in the spectra measured by the zero-degree arrangement.

We would expect further experimental studies on the angular dependence of the spectral distributions to obtain a deeper understanding of the alignment or orientation of the doubly excited states produced by the collision process.

F. Production of Rydberg states of high-*n* and high-angular momentum states

One of the most remarkable features found in the autoionization spectra of doubly excited He produced by the double-electron-capture processes of He^{2+} from Ba or other alkaline-earth atoms is that the autoionization peaks from the high-Rydberg states of large principal quantum numbers $n\geqslant 7$ have remarkable intensities up to very close to the series limit for both the $(2lnl')$ and $(3lnl')$ states.

Bordenave-Montesquieu *et al.* observed the high-Rydberg series populated in the $(3lnl')$ states in doubly excited He-like ions produced by the collisions $N^{7+}+He$ and $Ne^{10+}+He$ at $10q$ keV energies [21]. In order to interpret the experimental results, they proposed an ingenious hypothesis based on a sort of post-collisional effect, which was called the auto-transfer to Rydberg states ATR effect [21,57]. The basic idea was that high-Rydberg states were fed from the quasisymmetrical doubly excited states initially populated, which was promoted by the post-collisional effect. For instance, they interpreted that the enhancement of the intensities of the $(3lnl')$ Rydberg lines $(n>9)$ was brought, by virtue of a sort of PCI effect, from the symmetrical $(4l4l')$ states that were preferably populated in the same energy range by the double-electron-capture process. In addition, the enhancement of the high-angular momentum states was interpreted as a Stark deformation of the Rydberg orbit by the Coulomb field of the receding ion.

At present, it is not clear whether these mechanisms are sufficient to interpret the present experimental findings, although they would be one of candidates. The energy overlap between the $(2lnl')$ states and the symmetrical $(3l3l')$ states, and energy overlap between the $(3lnl')$ and the $(4l4l')$ states, are quite inadequate for doubly excited states in neutral He to promote the ATR effect.

Further investigations might be expected to elucidate mechanisms that control the electron stabilization and competition between autoionization and fluorescence yields of the Rydberg states, which follow the double-electron-capture process.

IV. SUMMARY AND CONCLUSIONS

In the present paper, we report experimental results of ejected electron spectra caused by the autoionization of the doubly excited states in He by means of zero-degree electron spectroscopy. The excited He was formed in the slow collisions of He^{2+} ions with Ba atoms.

(1) Spectra attributable to the autoionization $He^{**}(2lnl')\rightarrow He^{+}(1s)$ and $He^{**}(3lnl')\rightarrow He^{+}$ $(2s$ or $2p)$ were observed. Most peaks and structures in the spectra have been identified by comparing them with results of theoretical calculations.

(2) In the spectra for the $(2lnl')$ states, the ${}_2(1,0)_2^{+}\,{}^3P^o$ and ${}_2(1,0)_3^{+}\,{}^3P^o$ states were clearly observed. No other peaks corresponding to triplet states were found in both spectra. This phenomenon was observed for Ba and Sr targets and not for Ca and Mg. We have no definite explanation for this phenomenon yet.

(3) In both spectra, doubly excited states of high-angular momenta such as ^1D, ^1F, or ^1G terms were observed predominantly over the ^1P and ^1S states, unlike the spectra produced by photon, electron, or ion impacts on neutral He atoms. Intensity distributions for individual doubly excited states in the present spectra are also quite different from those produced by means of the impact processes.

(4) The species of doubly excited states and their population distribution observed in the present spectra is, in general, consistent with those of He-like ions produced by double-electron-capture collisions of fully stripped ions with atomic targets, except for a few exceptions. For instance, the ${}_2(1,0)_3^{-}\,{}^1P^o$ state was clearly observed for the He-like ions, while it is known to be observed only very weakly in the case of particle impact on neutral He.

(5) In both spectra for the $(2lnl')$ and $(3lnl')$ series, the intensities of the autoionization lines for states of high-principal quantum numbers, do not decrease rapidly and keep rather high values with rising *n*, resulting in a steep cliff at the series limits. This feature was observed more notably for the higher-collision energies.

(6) From the collision energy dependence of the intensity distribution in the autoionization lines, the following features were found.

(a) The intensities of the lines for the $(3lnl')$ series are nearly one order of magnitude larger than those for the $(2nl')$ series at the collision energy of 40 keV. The intensity ratio of the $(3lnl')$ series relative to the $(2lnl')$ ones decreases as the collision energy decreases down to 20 keV, strongly by a factor of about three.

(b) The tendency of the favorable population for high-Rydberg states, i.e., the observation of a steep edge at the series limit, is reduced as the collision energy decreases.

(c) The intensity of the $^1D^e$ terms relative to that for $^1F^o$ appears to decrease as the collision energy decreases. The peaks attributable to the $^1F^o$ terms become predominant at the lowest collision energy 20 keV.

In order to understand these features, a theoretical study is in progress to interpret these propensity rules in connection with the consideration of the high polarizabilities of both the double excited He atom and the Ba target atom. Results of this study will be published before long.

In order to obtain more unique experimental information, we should perform systematic measurements of the angular dependence of the electron ejection in the autoionization, and thereby determine the differential cross sections for autoionization. To get the overall population distribution of individual states, high-resolution translational energy-gain spectroscopy of colliding ions, which proves its effectiveness in the single-electron transfer collision processes, are expected to be useful. A method to measure the radiative decay yields in doubly excited $^1P^o$ states in He, which recently proved to be successful in a photoexcitation process [58], may also be applied to doubly excited states produced by He^{2+} collisions.

[1] R. P. Madden and K. Codling, Phys. Rev. Lett. **10**, 516 (1963); J. Opt. Soc. Am. **54**, 2683 (1964); Astrophys. J. **141**, 36 (1965).

[2] J. A. Simpson and S. R. Mielczarek, J. Chem. Phys. **39**, 1606 (1963); J. A. Simpson, S. R. Mielczarek, and J. Cooper, J. Opt. Soc. Am. **54**, 269 (1964); J. A. Simpson, G. E. Chemberlain, and S. R. Mielczarek, Phys. Rev. **139**, A1039 (1965).

[3] M. E. Rudd, Phys. Rev. Lett. **13**, 503 (1964); **15**, 580 (1965).

[4] H. Suzuki, A. Konishi, M. Yamamoto, and K. Wakiya, J. Phys. Soc. Jpn. **28**, 534 (1970); H. Suzuki, T. Takayanagi, K. Wakiya, and Y. Jimbo, Abstracts of Contributed Papers of the Fourth International Conference on Atomic Physics, Heidelberg, 1974, pp. 473–476 (unpublished).

[5] N. Oda, F. Nishimura, and S. Tahira, Phys. Rev. Lett. **24**, 42 (1970).

[6] K. Siegbahn *et al., ESCA Applied to Free Molecules* (North Holland, Amsterdam, 1969), p. 26.

[7] D. W. Lindle, T. A. Ferrett, P. A. Heimann, and D. A. Shirley, Phys. Rev. A **36**, 2112 (1987).

[8] M. Domke, C. Xue, A. Puschmann, T. Mandel, E. Hudson, D. A. Shirley, G. Kaindl, C. H. Greene, H. R. Sadeghpour, and H. Peterson, Phys. Rev. Lett. **66**, 1306 (1991).

[9] M. Domke, G. Remmers, and G. Kaindl, Phys. Rev. Lett. **69**, 1171 (1992).

[10] M. Zubek, G. Dawber, R. I. Hall, L. Avalidi, K. Ellis, and G. C. King, J. Phys. B **24**, L337 (1991).

[11] D. R. Herrick and O. Sinanoglu, Phys. Rev. A **11**, 97 (1975).

[12] C. D. Lin, *Advances in Atomic and Molecular Physics* (Academic, New York, 1986), Vol. 22, pp. 77–142.

[13] C. D. Lin, *Review of Fundamental Processes and Applications of Atoms and Ions* (World Scientific, Singapore, 1993), pp. 357–401.

[14] J. P. Giese M. Schulz, J. K. Swenson, H. Schoene, M. Benhenni, S. L. Varghese, C. R. Vane, P. F. Dittner, S. M. Shafroth, and S. Datz, Phys. Rev. A **42**, 1231 (1990).

[15] P. J. Hicks, S. Cvejanovic, J. Comer, F. J. Read, and J. M. Sharp, Vacuum **24**, 573 (1974); F. J. Read, Radiat. Res. **64**, 23 (1975).

[16] R. B. Rarker and H. W. Berry, Phys. Rev. **151**, 14 (1966).

[17] M. Mack, J. H. Nijland, P. v. d. Straten, A. Niehaus, and R. Morgenstern, Phys. Rev. A **39**, 3846 (1989).

[18] H. A. Sakaue, Y. Kanai, K. Ohta, M. Kushima, T. Inaba, S. Ohtani, K. Wakiya, H. Suzuki, T. Takayanagi, T. Kambara, A. Danjo, M. Yoshino, and Y. Awaya, J. Phys. B **23**, L401 (1990).

[19] S. Ohtani, Y. Kanai, I. Yamada, H. A. Sakaue, Y. Awaya, T. Kambara, T. Nabeshima, N. Nakamura, H. Suzuki, T. Takayanagi, K. Wakiya, A. Danjo, and M. Yoshino, Nucl. Instrum. Methods Phys. Res. B **53**, 383 (1991).

[20] H. A. Sakaue, Y. Awaya, A. Danjo, T. Kambara, Y. Kanai, T. Nabeshima, N. Nakamura, S. Ohtani, H. Suzuki, T. Takayanagi, K. Wakiya, I. Yamada, and M. Yoshino, J. Phys. B **24**, 3787 (1991).

[21] A. Bordenave-Montesquieu, P. Moretto-Capelle, A. Gonzalez, M. Benhenni, H. Bachau, and I. Sanchez, J. Phys. B **27**, 4243 (1994).

[22] J. Y. Chesnel, H. Merabet, B. Sulik, F. Fremont, C. Bedouet, X. Husson, M. Grether, and N. Stolterfoht, Phys. Rev. A **58**, 2935 (1998).

[23] P. Moretto-Capelle, D. Bordenave-Montesquieu, A. Bordenave-Montesquieu, and M. Benhenni, J. Phys. B **31**, L423 (1998).

[24] K. Iemura, F. J. Currell, S. Ohtani, K. Kitazawa, M. Koide, H. Suzuki, M. Sekiguchi, S. Machida, T. Takayanagi, and K. Wakiya, Phys. Scr., T **73**, 205 (1997).

[25] Y. Kanai, K. Iemura, and X.-M. Tong, in *The Physics of Electronic and Atomic Collisions*, edited by Y. Itikawa, H. Tanaka, A. Yagishita, and M. Matsuzawa, AIP Conf. Proc. No. 500 (AIP, Melville, NY, 2000), p. 606–615.

[26] M. Sekiguchi, Y. Ohshiro, M. Fujita, T. Yamazaki, Y. Yamashita, Y. Isoya, T. Yamada, and A. Kitagawa, *Proceedings of the 12th International Conference On Cyclotron and Their Applications* (World Scientific, Singapore, 1992), pp. 326–329.

[27] N. Nakamura, H. Ida, Y. Matsui, K. Wakiya, T. Takayanagi, M. Koide, F. J. Currell, S. Kitazawa, H. Suzuki, S. Ohtani, U. I. Safronova, and M. Sekiguchi, J. Phys. B **28**, 4743 (1995).

[28] N. Nakamura, Y. Awaya, F. J. Currell, T. Kambara, Y. Kanai, S. Kitazawa, M. Koide, S. Ohtani, U. I. Safronova, H. Suzuki, T. Takayanagi, and K. Wakiya, J. Phys. B **29**, 1995 (1996).

[29] S. Kitazawa, K. Tanabe, S. Machida, Y. Matsui, H. Ida, T. Takayanagi, K. Wakiya, K. Iemura, F. Currell, S. Ohtani, H. Suzuki, M. Sekiguchi, and U. I. Safronova, J. Phys. B **31**, 3233 (1998).

[30] N. Stolterfoht, Phys. Rep. **146**, 315 (1987).

[31] L. O. Werme, T. Bergmark, and K. Siegbahn, Phys. Scr. **6**, 141 (1972).

[32] E. Lindroth, Phys. Rev. A **49**, 4473 (1994).

[33] Y. K. Ho, Phys. Rev. A **23**, 2137 (1981).
[34] Y. K. Ho, Phys. Rev. A **34**, 4402 (1986).
[35] Y. K. Ho and A. K. Bhatia, Phys. Rev. A **44**, 2875 (1991).
[36] Y. K. Ho, Z. Phys. D: At., Mol. Clusters **21**, 191 (1991).
[37] Y. K. Ho, Phys. Rev. A **48**, 3598 (1993).
[38] J. Z. Tang, S. Watanabe, and M. Matsuzawa, Phys. Rev. A **46**, 2437 (1992).
[39] J. Z. Tang, S. Watanabe, and M. Matsuzawa, Phys. Rev. A **46**, 3758 (1992).
[40] T. Morishita, K. Hino, S. Watanabe, and M. Matsuzawa, Phys. Rev. A **53**, 2345 (1996).
[41] L. Lipsky, R. Anania, and M. J. Conneely, At. Data Nucl. Data Tables **20**, 127 (1977).
[42] M. Boudjema, M. Cornille, J. Dubau, P. Moretto-Capelle, A. Bordenave-Montesquieu, P. Benoit-Cattin, and A. Greizes, J. Phys. B **24**, 1695 (1991); **24**, 1713 (1991).
[43] P. van der Straten and R. Morgenstern, Phys. Rev. A **34**, 4482 (1986).
[44] Y. K. Ho, J. Phys. B **12**, 387 (1979).
[45] Y. K. Ho and J. Callaway, J. Phys. B **18**, 3481 (1985).
[46] Y. K. Ho, Phys. Rev. A **44**, 4154 (1991).
[47] Y. K. Ho and A. K. Bhatia, Phys. Rev. A **44**, 2895 (1991).
[48] Y. K. Ho and A. K. Bhatia, Phys. Rev. A **47**, 2628 (1993).
[49] Y. K. Ho, Phys. Rev. A **48**, 3598 (1993).
[50] Y. K. Ho and A. K. Bhatia, J. Phys. B **30**, 3597 (1997).
[51] A. K. Bhatia and Y. K. Ho, J. Phys. B **31**, 3307 (1998).
[52] N. Koyama, H. Fukuda, T. Motoyama, and M. Matsuzawa, J. Phys. B **18**, L331 (1986).
[53] N. Koyama, A. Takafuji, and M. Matsuzawa, J. Phys. B **22**, 553 (1989).
[54] S. J. Brotton, S. Cvejanovic, F. J. Currell, N. J. Bowring, and F. H. Read, Phys. Rev. A **55**, 318 (1997).
[55] T. Watanabe, X. M. Tong, S. Ohtani, K. Iemura, Y. Kanai, and H. Suzuki, in *Abstracts of Contributed Papers*, *XXIth International Conference on the Physics of Electronic and Atomic Collisions*, Sendai, 1999, edited by Y. Itikawa, K. Okuno, H. Tanaka, A. Yagishita, and M. Matsuzawa (unpublished), p. 549.
[56] Z. Chen and C. D. Lin, J. Phys. B **24**, 4231 (1991).
[57] P. Roncin, M. N. Gaboriaud, M. Barat, A. Bordenave-Montesquiu, P. Morreto-Capelle, M. Benhenni, H. Bachau, and C. Harel, J. Phys. B **26**, 4181 (1993).
[58] K. M. Odling-Smee, E. Sokell, P. Hammond, and M. A. MacDonald, Phys. Rev. Lett. **84**, 2598 (2000).